JOURNAL OF MATERIALS SCIENCE 33 (1998) 2691–2700

Microstructural evaluation of molybdenum-containing stainless steel weld metals by a potentiostatic etching technique

M. G. PUJAR, R. K. DAYAL, T. P. S. GILL*
*Metallurgy Division, and *Materials Development Division, Indira Gandhi Centre for Atomic Research, Kalpakkam 603 102, India*
E-mail: pujar@igcar.ernet.in

S. N. MALHOTRA
Department of Metallurgical Engineering and Materials Science, Indian Institute of Technology, Bombay 400 076, India

Microstructure of austenitic stainless steel weld metals is complicated by the presence of delta-ferrite and microsegregated regions rich in chromium and molybdenum, as well as other minor alloying elements such as sulphur and phosphorus at the δ/γ interphase boundaries. Detailed microstructural studies are required in order to establish correlation between various metallurgical as well as electrochemical corrosion properties with the weld metal microstructure. The conventional chemical etching technique was found to be inadequate in revealing different microconstituents. A powerful potentiostatic etching technique was used to reveal not only ferrite but also different microconstituents that had different specific electrochemical potentials at which they dissolved. This paper describes the weld metal microstructure developed by the addition of molybdenum (4.16–5.83 wt%) to type 316 stainless steel weld metals during Tungsten Inert Gas (TIG) welding with different heat inputs.

1. Introduction

Austenitic stainless steel weld metals of 300 series generally contain 2%–10% delta-ferrite in order to avoid the problem of solidification cracking [1]. The amount and morphology of the delta-ferrite is a sensitive function of the weld chemistry (Cr_{eq}/Ni_{eq}) ratio. It is well known that the cycle of rapid heating and cooling that occurs during the welding process affects the microstructure and surface composition of welds. Heat input and welding technique affect the solidification behaviour of weld metals. The microsegregation of chromium and molybdenum during weld solidification and cooling in type 316 and type 316L weld metal has been extensively studied by a number of workers [2–6]. They concluded that microsegregation of chromium and particularly that of molybdenum [3, 4] was found to be much higher at the δ/γ interphase boundaries. The segregated molybdenum was reported to be more detrimental for uniform corrosion of high-alloyed austenitic stainless steels [7]. Hence a careful metallographic examination of welds not only reveals how perfect are the weld joints and the effects of welding parameters on the joints, but it also helps in establishing the structure–property correlation [8].

Microstructural studies of these weld metals by conventional chemical etching do not provide adequate information of the microstructural complexities. Potentiostatic etching (electrochemical dissolution at constant applied potential) was found to be very useful in this context. This technique can be effectively used to locate various microstructural regions in the weld metal that differ in chemical composition as well as electrochemical properties. Various phases, segregated regions and microconstituents of the weld metal become electrochemically activated (or attack is initiated) at different electrochemical potentials, depending upon their chemical composition. Because the electrode reactions take a finite time to establish a steady state, during anodic polarization such a steady state is never obtained and their behaviour is partially or totally masked. Also, the overwhelming activity of the major phase (or matrix) decides the overall shape of the dynamic polarization curve. In an alloy containing two or more phases, each phase has a certain characteristic polarization curve and by comparing these, it is possible to choose a potential at which a particular phase is preferentially etched, keeping the other phases in the passive condition [9]. Potentiostatic etching at different potentials then becomes a useful tool in finding out those regions that cannot be detected by means of ordinary chemical etching and which are masked during anodic polarization. Cihal and Prazak [10] studied the electrochemical aspects of different stainless steels, the chemical compositions of which matched those of

delta-ferrite, austenite and sigma in 5% H_2SO_4 containing 0.1 $g l^{-1}$ NH_4SCN. They established polarization diagrams of these alloys and presented potential values in the active as well as transpassive regions to be used for potentiostatic etching in this medium. True electrochemical behaviour of ferrite and sigma would be dependent on the actual weld chemistry as well as on the ferrite morphology, and alloys of similar compositions might not represent their behaviour. But such studies were not carried out on the austenitic stainless steel weld metals. The investigations by Gooch *et al.* [9] on type 304 and type 316 weldments, prepared with different welding techniques having different chemical compositions and ferrite contents, concentrated largely on determination of potentiostatic polarization curves of these weldments in 20% H_2SO_4 containing 0.1 $g l^{-1}$ NH_4SCN. They quantified the dissolution of the weldments at different potentials and tried to find out the exact or static electrochemical potentials of different parameters such as active peak and passivation potential, etc. They dealt more with the potentiostatic etching aspects of the weldment as a whole. Also, in a recent work, Marshall and Gooch [11] have made use of static and dynamic values of passivation potentials and have tried to correlate the arithmetic difference between these two with the segregation factors for chromium, molybdenum and nitrogen for various austenitic stainless steels with a wide range of chromium, nickel and molybdenum concentrations.

It has been documented that ferrite is attacked at an active potential compared to austenite [12]. But in a dynamic polarization curve of a weld metal, the dissolution of ferrite is not clearly indicated. The microstructural details punctuated between austenite peak and delta-ferrite peak potentials have not been explored. These facts suggested that the static dissolution behaviour of weld metal is not sufficiently known. Weld metal corrosion of different microconstituents and phases could be well appreciated by studying the fundamental anodic polarization curves obtained in 1N H_2SO_4 medium for pure chromium metal [13], that of alloys with various amounts of chromium additions [14] (at fixed nickel concentrations) and of alloys where molybdenum is added to nickel-based alloys [15]. In the present investigations, the microstructural features of weld metals prepared by adding molybdenum have been studied by employing the potentiostatic etching technique. Extensive optical microscopic observations that were carried out are discussed.

2. Experimental procedure

2.1. Weld metal preparation

To prepare weld metal samples with known and controlled additions of alloying elements, a novel technique was employed. This technique is known as "Stationary Arc TIG Welding" (SATIG). Under standardized welding conditions, TIG welding was carried out at a spot on the work-piece by keeping the arc stationary for a fixed time duration, which could give required weld penetration. In the present work, 316 stainless steel plate of known chemical composition was used for welding. A plate of 100 mm × 100 mm × 25 mm size was used in order to dissipate the heat during welding. Welding conditions (Table I) were standardized by preparing weld metals without any alloying element addition. Ultra high purity argon gas was used for shielding the weld puddle from oxidation. Addition of alloying elements during welding was accomplished by inserting the accurately weighed wire pieces (of ultra high purity) of molybdenum by a ceramic rod to avoid any contamination. Melting the plate for 75 s resulted in the weld metal with 15 mm diameter and 7–8 mm penetration. Four weld pads each with 50 mg and 140 mg molybdenum additions were prepared under these conditions.

TABLE I Welding conditions for stationary arc TIG welding

Welding current	200 A
Arc gap	3 mm
Argon flow rate	6 l min^{-1}
Welding voltage	20 V
Welding time	75 s

2.2. Change in the heat input

In order to alter the heat input, a different technique was adopted. Heat input could be changed by changing the arc strike time. Four weld pads from each set prepared by the technique given above were used to obtain weld metals with different heat inputs but having the same chemical composition. The tungsten electrode tip was kept exactly at the centre of the weld (with 75 s melting time). Except for current, voltage and arc strike time, all the welding conditions were the same as given in Table I. A stationary TIG arc was struck on these four welds for 5, 10, 15 and 20 s (at 100 A), respectively. The technique for the addition of alloying elements during stationary arc TIG welding and the weld pad thus prepared, are shown in Fig. 1. Weld metals were carefully machined from the plate to avoid any base metal contamination.

2.3. Heat input measurement and calculation

A standardized technique of measurement of the cooling curves during welding was adopted to determine the heat input values. As in the stationary arc TIG welding technique, where the torch is stationary, an indirect method of calculation of heat input was followed. This method consisted of measurement of cooling curves during autogenous welding (moving torch) at known heat input values. From these measurements, a standard plot of heat input values versus cooling time between two fixed temperatures was prepared, which was used as a calibration curve. Cooling curves were measured during stationary arc TIG welding for different arc strike times. The cooling curves obtained from these experiments would yield cooling times and from the above calibration curve, one could obtain heat input values. In order to

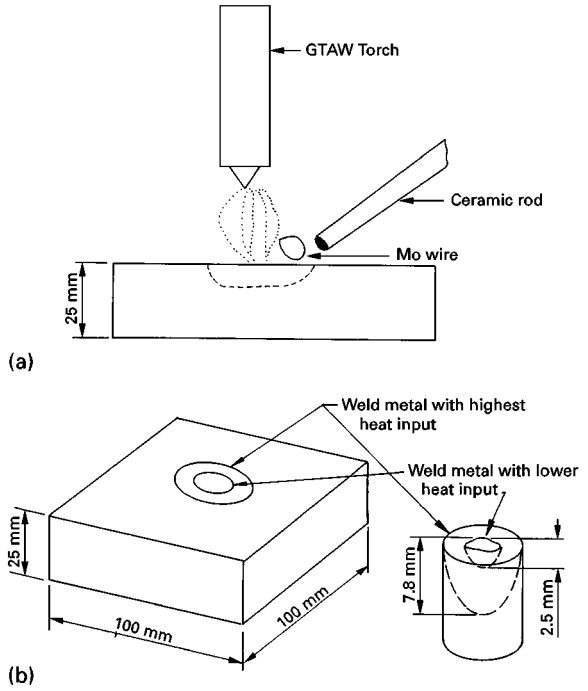

Figure 1 (a) Representation of the stationary arc TIG (SATIG) welding by adding molybdenum wire. (b) A 316 SS weld pad showing the location of the weld metals and the machined weld metal.

measure the cooling curves, a thermocouple made of tungsten–5% rhenium/tungsten–26% rhenium was employed. One end of the leads of the thermocouple was connected to the strip chart recorder while the other end was kept ready for plunging into the molten pool during welding. Autogenous welding (100 A, 12 V, 3 mm arc gap) was carried out on 25 mm thick plate at heat input values of 0.58, 0.72, 0.96 and 1.44 kJ mm^{-1}, respectively by varying the torch travel speed. During autogenous welding the thermocouple end was plunged into the weld pool as soon as the torch passed by for measurement of cooling curves. In the case of stationary arc TIG welding, the measurement of the cooling curves was accomplished in a similar manner by plunging the thermocouple end into the molten pool immediately after the arc was extinguished.

In order to determine the chemical composition of these welds, a number of welds with 75 s melting time were prepared and drilled (up to a depth of 3 mm only) to collect weld chips. These were degreased and then subsequently used for wet chemical analysis.

2.4. Delta-ferrite measurement

Delta-ferrite measurement was carried out on the polished weld metals (~ 1 μm finish) by a Magnegage. For a weld with the highest welding time of 75 s, because the weld metal area was large, a total of 40 readings was taken, but in the case of weld metals with different heat input values, where the specimen area was small (~ 0.3 cm^2), a total of 25 readings was taken, in order to arrive at an average delta-ferrite value.

2.5. Microstructural characterization

2.5.1. Chemical etching technique

Normally austenitic stainless steel weld metals are etched in Murakami reagent (boiling solution of 10 g of potassium ferricyanide + 10 g potassium hydroxide) for about 3 min, wherein only weld metal delta-ferrite is attacked. All the welds polished up to fine diamond (~ 1 μm finish) were etched in this reagent, rinsed in distilled water, dried and then observed under an optical microscope to study delta-ferrite morphology.

2.5.2. Potentiostatic etching technique

This technique involved preparations of the weld metal specimen by polishing up to fine diamond finish, cleaning free from any grease and oil, and finally rinsing with doubly distilled water. A solution of 0.5 M H_2SO_4 + 0.1 g l^{-1} NH_4SCN was prepared in double distilled water. This solution was deaerated by passing ultra-high purity argon gas through it for 1 h before the immersion of the specimen. Throughout etching experiments, the solution was continuously purged. After immersion the specimen was cathodically cleaned by impressing a potential of − 800 mV(SCE) for 1 min. After surface cleaning, the potential at which etching was to be carried out was impressed immediately, in order to avoid any corrosion attack at open circuit potential (OCP). In order to obtain accurate OCP values an initial impressed potential of − 440 mV(SCE) was selected. Time of the etching varied at every potential step, depending upon the dissolution current. Subsequent to etching the specimen was removed, rinsed in distilled water and dried. At every etching step, careful optical microscopic observations were made to ascertain which phases or microconstituents were attacked. The impressed potential was changed in the noble direction in steps of 20 mV until the specimen passivated. All the potentiostatic etching experiments were carried out using a Wenking STP 84 potentiostat.

3. Results and discussion

Chemical compositions of all the weld metals with and without the addition of molybdenum are given in Table II. Chemical compositions of the weld with 75 s melting time and those prepared at different heat

TABLE II Chemical composition of the weld metals (wt%)

Element	Weld metal type		
	Without any addition	Mo1	Mo2
Carbon	0.039	0.039	0.041
Silicon	0.61	0.60	0.57
Manganese	1.44	1.40	1.44
Sulphur	0.020	0.019	0.020
Phosphorus	0.020	0.025	0.027
Chromium	16.81	16.80	16.63
Nickel	10.61	11.07	11.23
Molybdenum	2.42	4.16	5.83

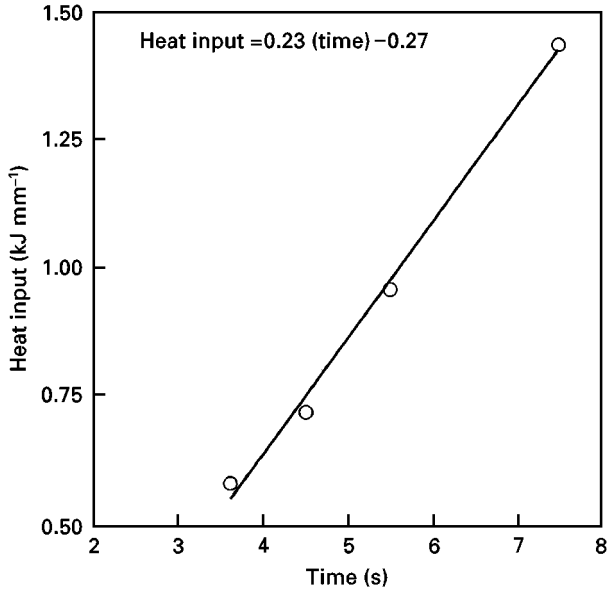

Figure 2 Heat input versus cooling time plot for autogenous TIG welding on 25 mm plate.

inputs were assumed to be the same for a given set of specimens. Chemical composition of the weld metal without any elemental addition has been given for reference. By addition of 50 mg and 140 mg molybdenum, the initial concentration of molybdenum (2.42 wt% without any elemental addition) has been changed to 4.16 wt% (1.74 wt% increase) and 5.83 wt% (3.41 wt% increase), respectively. The carbon, nitrogen and nickel levels were found to be unchanged by the addition of molybdenum during welding. The weld metal specimens with 50 and 140 mg Mo additions are designated **Mo1** and **Mo2**, respectively.

3.1. Heat input values

In our experiments, the temperature interval from 1000 °–500 °C was chosen to determine the cooling times. The calculated cooling times for autogenous welds at different heat inputs when plotted (Fig. 2) gave a best fit line with an equation as

$$\text{Heat input (kJ mm}^{-1}) = 0.23\ (\text{Cooling time, s}) - 0.27 \quad (1)$$

Under the conditions of the same stationary arc TIG welding parameters and the same plate thickness, heat input values can be calculated from Equation 1. The equivalent heat input values for 5, 10, 15, 20 s arc strike times were calculated by using Equation 1 and were found to be 0.36, 0.56, 0.85 and 1.00 kJ mm^{-1}, respectively. These can be termed the equivalent heat input (EHI) because the TIG arc was stationary.

3.2. Microstructural studies

3.2.1. Chemical etching

The mode of solidification is dependent on the Cr_{eq}/Ni_{eq} ratio. Many workers have presented different formulae to calculate this ratio. The Cr_{eq}/Ni_{eq} ratios calculated by using different formulae have been presented in Table III. The mode of solidification was found to be primary ferritic as all the specimens had Cr_{eq}/Ni_{eq} ratios higher than 1.5 [16]. The microstructure of solidified austenitic stainless steel welds is characterized according to the morphology of the ferrite present. Development of final microstructure is dependent on several welding and metallurgical conditions. The complexity of many of these microstructures has led to considerable confusion in the interpretation of the weld microstructure evolution. Recently, different ferrite morphologies have been classified properly by David [17] and have been discussed by Brooks and Thompson [18] in detail. Essentially, skeletal ferrite morphology was observed for Mo1 weld metals prepared at lower heat inputs with increased interconnectivity (Fig. 3a). Subsequently, the skeletal morphology changed to a lathy one with equispaced ferrite particles (Fig. 3b). Predominantly lathy ferrite was observed in Mo2 weld metals (Fig. 4a, b). Widmanstätten austenite was noted in one of the specimens (Fig. 4c).

TABLE III Cr_{eq}/Ni_{eq} ratios by using different formulae

Weld metal type	Suuatala's Cr_{eq}/Ni_{eq} (a)	DeLong's Cr_{eq}/Ni_{eq} (b)	WRC-92 Cr_{eq}/Ni_{eq} (c)
Without any addition	1.71	1.50	1.53
Mo1	1.83	1.58	1.61
Mo2	1.96	1.66	1.69

(a) Suutala's $Cr_{eq}/Ni_{eq} = \dfrac{Cr + 1.37\,Mo + 1.5\,Si + 2\,Nb + 3\,Ti}{Ni + 0.31\,Mn + 22C + 14.2\,N + Cu}$

(b) DeLong's $Cr_{eq}/Ni_{eq} = \dfrac{Cr + Mo + 1.5\,Si + 0.5\,Nb}{Ni + 0.5\,Mn + 30\,(C + N)}$

(c) WRC-1992 $Cr_{eq}/Ni_{eq} = \dfrac{Cr + Mo + 0.7\,Nb}{Ni + 35\,C + 20\,N + 0.25\,Cu}$

Note: Nitrogen concentration was assumed to be 0.03 wt% in the above specimens.

3.2.2. Delta-ferrite content

The ferrite contents of the weld metals are presented in Table IV. It was observed that the ferrite contents of the welds with lower heat input values generally varied in a range marked by the ferrite content of the highest heat input weld metal ± 2 Ferrite Number (FN, a unit of delta-ferrite). This variation in ferrite content is not considered significant.

3.2.3. Potentiostatic etching

In the present study, the weld metal specimens Mo1 and Mo2 showed actual weld metal molybdenum concentrations of 4.16 wt% and 5.83 wt%, respectively. But during potentiostatic etching experiments the slight difference in molybdenum level did not show a significant difference in microstructural characteristics of these specimens. Fig. 5a–l are micrographs obtained during weld metal etching at different potentials starting from OCP and moving in the noble

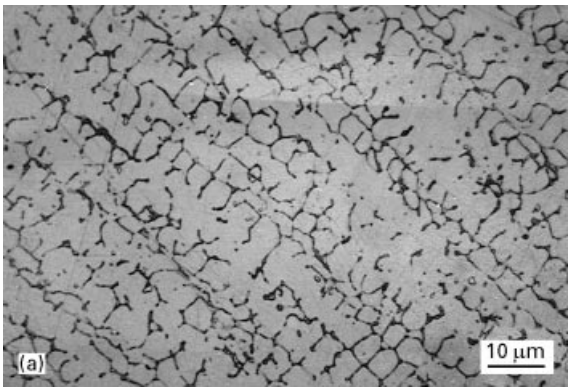

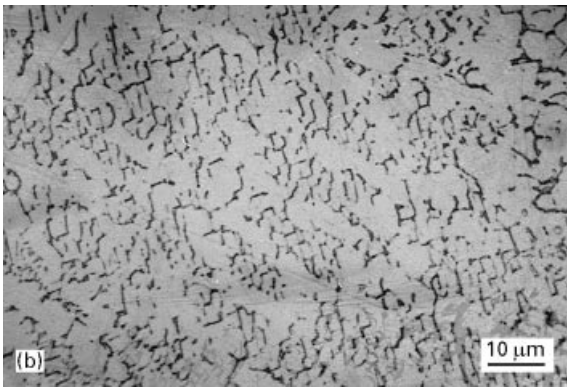

Figure 3 Microstructure of Mo1 weld metals in the as-welded condition showing (a) interconnectivity of the ferrite, (b) lathy ferrite. Etched in Murakami's reagent.

direction, until the specimen was passivated. Attack on delta-ferrite commenced from -440 mV(SCE) and lasted until -340 mV(SCE), but attack on different microconstituents was observed at different potentials (Fig. 5a–g). The ferrite which was enriched in chromium was attacked at very active potentials [9, 10]. Essentially, it was the chromium enrichment in ferrite that led to such an attack which took place just after the OCP was crossed. It is well documented that increase in ferrite content also shifts the weld metal OCP in the active direction [9]. These specimens had ferrite contents as high as 8–10 FN. Fig. 5a shows the clear attack on the ferrite network as well as black zones spread over several places which were also attacked. These were the zones where chromium and, to a certain extent, molybdenum would have segregated during weld solidification, as this weld was prepared at the lowest heat input (0.36 kJ mm^{-1}) having the highest cooling rate. These black zones appeared due to the redistribution of solute elements during solidification. This kind of redistribution on a finer scale than that of the dendrite arm spacing, is called microsegregation. Microsegregation across the dendrite has been extensively studied by Lippold and Savage [19] on type 304 GTA welds. Their investigation implied that there were two transients of concentrations of solutes; one in the beginning and one at the far end, and the concentration profile at the centre connecting these two transients was uniform. This explanation was not accepted, as several factors including the solid-state diffusion of alloying elements were ignored. Brooks and Baskes [20] also addressed the topic of microsegregation and concluded that there was a monotonic increase in the composition profile across the dendrite for some binary alloys, the view which received wide acceptance. Essentially, these black zones could be attributed to the areas where delta-ferrite existed as soon as the weld pool solidified. During subsequent cooling, the majority of these areas were transformed

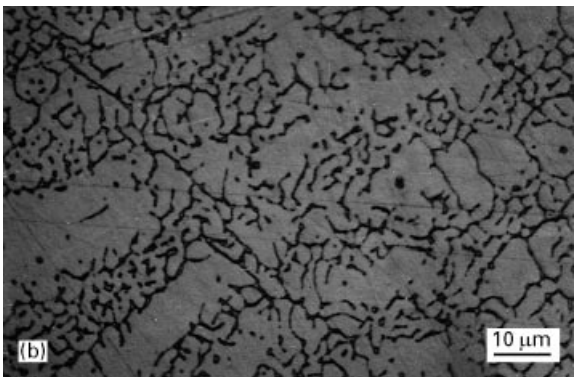

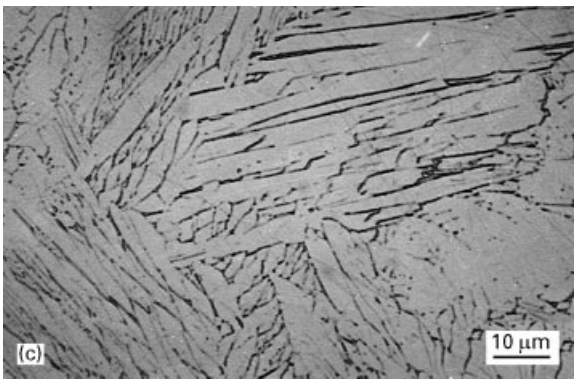

Figure 4 Microstructure of Mo2 weld metals in the as-welded condition showing (a, b) lathy ferrite, and (c) Widmanstätten austenite. Etched in Murakami's reagent.

TABLE IV Delta-ferrite contents of weld metals with different heat inputs (FN)

Heat input (kJ mm^{-1})	Without any addition	Mo1	Mo2
0.36	3.4 ± 0.4	8.3 ± 0.2	9.6 ± 0.3
0.56	4.0 ± 0.3	6.6 ± 0.2	9.2 ± 0.6
0.85	5.0 ± 0.1	7.0 ± 0.3	8.9 ± 0.3
1.00	6.5 ± 0.2	8.7 ± 0.5	8.7 ± 0.3
Weld with 75 s meltig time	4.2 ± 0.4	6.1 ± 0.5	10.3 ± 0.6

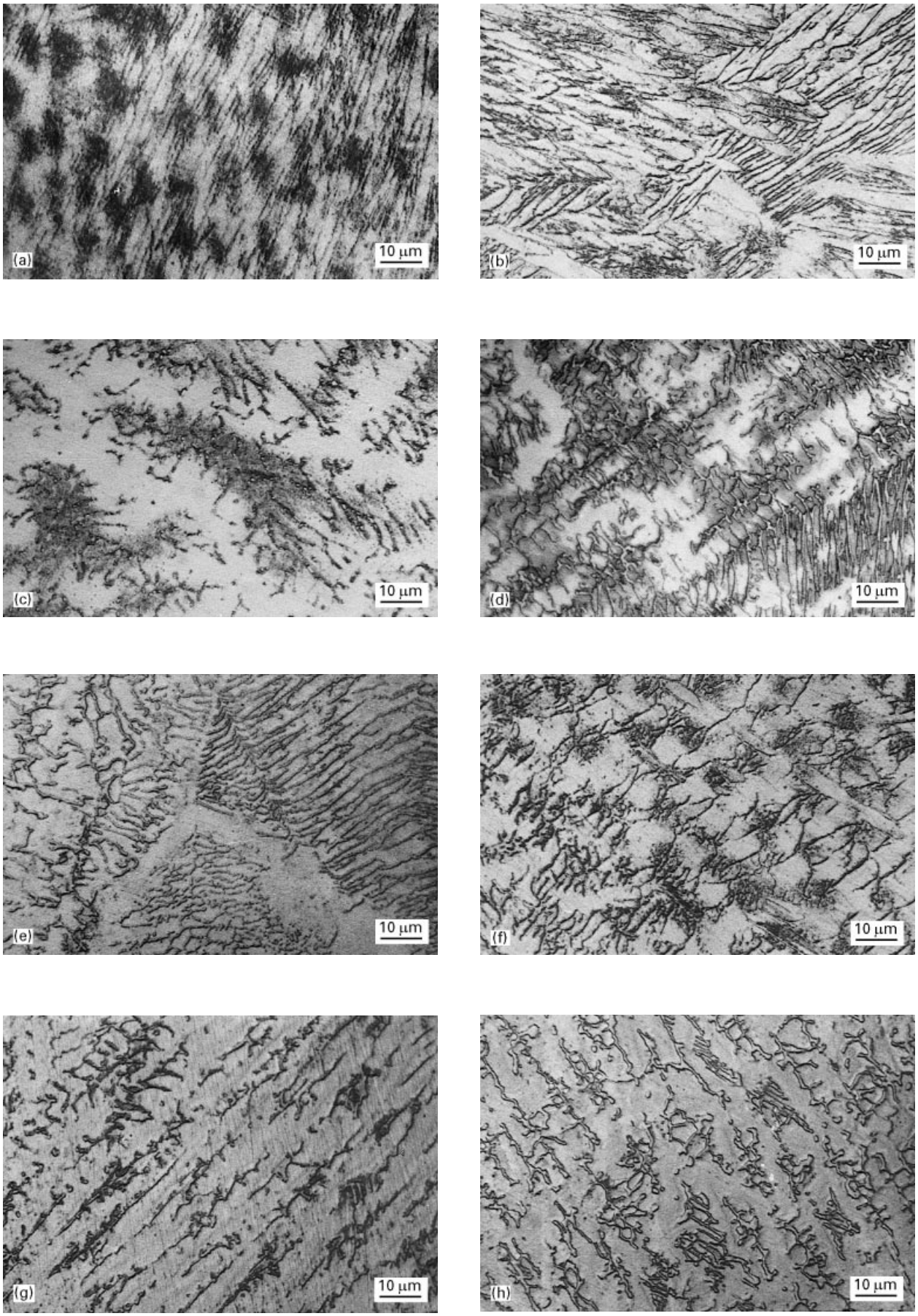

Figure 5 Photomicrographs after potentiostatic etching in 0.5 M $H_2SO_4 + 0.1\ g\,l^{-1}$ NH_4SCN at different active potentials. Weld metal specimens with 4.16–5.83 wt% Mo. (a) Mo2, 0.36 kJ mm^{-1}, − 440 mV(SCE); (b) Mo2, 0.85 kJ mm^{-1}, − 420 mV(SCE); (c) Mo2, 0.85 kJ mm^{-1}, − 420 mV(SCE); (d) Mo1, 0.36 kJ mm^{-1}, − 400 mV(SCE); (e) Mo1, 0.56 kJ mm^{-1}, − 380 mV(SCE); (f) Mo2, 1.00 kJ mm^{-1}, − 360 mV(SCE); (g) Mo1, 0.85 kJ mm^{-1}, − 340 mV(SCE); (h) Mo1, 1.00 kJ mm^{-1}, − 320 mV(SCE); (i) Mo2, 0.36 kJ mm^{-1}, − 300 mV(SCE); (j) Mo2, 0.85 kJ mm^{-1}, − 260 mV(SCE); (k) Mo2, 1.00 kJ mm^{-1}, − 240 mV(SCE); (l) Mo1, 0.36 kJ mm^{-1}, − 220 mV(SCE).

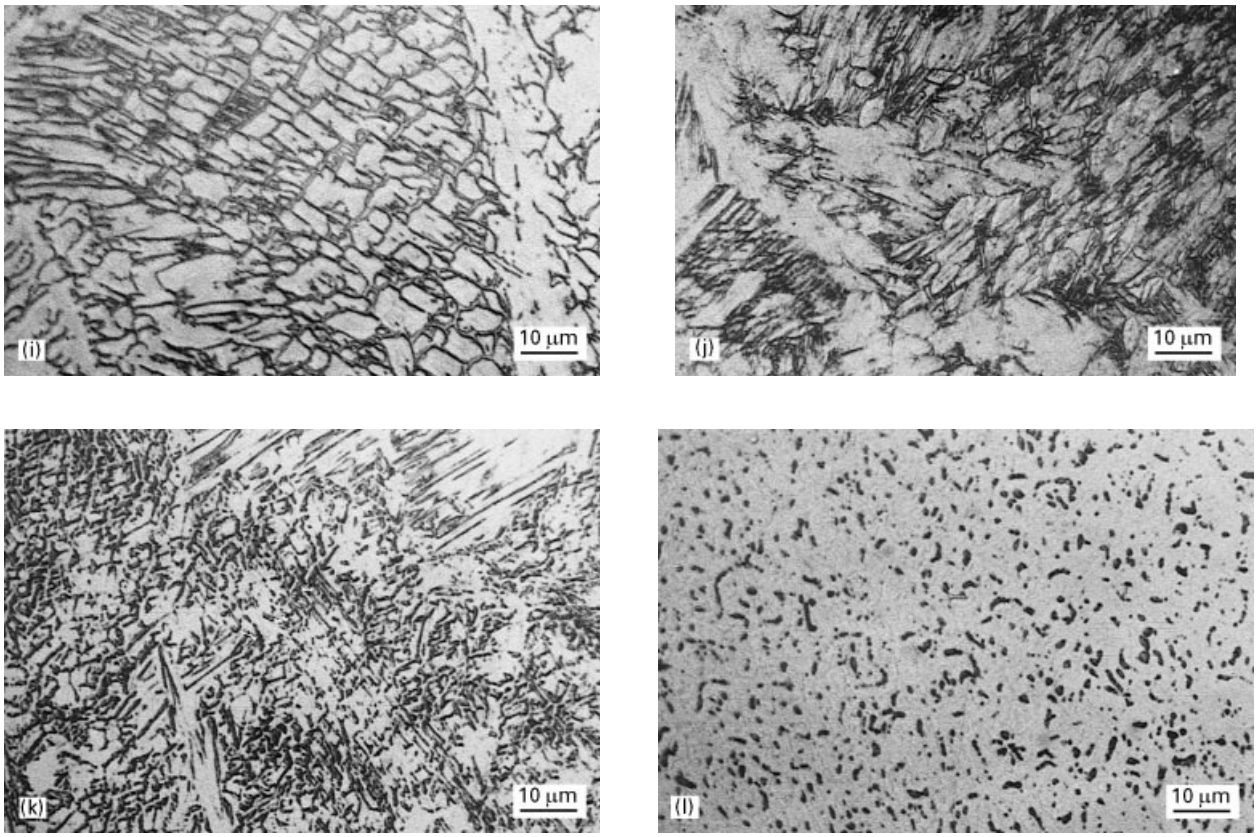

Figure 5 (continued).

to austenite by a solid-state diffusion mechanism. But as the cooling rate in these low heat input (0.36 kJ mm^{-1}) specimens was the highest, complete homogenization of the chromium did not take place, leaving these zones rich in chromium. Such a type of attack was observed even in Fig. 5c around ferrite. On careful observation of this micrograph it was found that there were many bright spots inside the primary ferrite core which were obviously passivated. This was due to the fact that at these spots the local chromium concentration was much higher than the average chromium concentration of the core; therefore, they were passivated at this potential. This can be well appreciated from Fig. 6 where the anodic polarization diagram of pure chromium in 1N H_2SO_4 is presented. It was observed that the attack on austenite was negligible from -440 to -400 mV(SCE). Attack on segregated zones could be observed up to -400 mV (SCE) wherein a major fraction of the ferrite was almost passivated (Fig. 5d). A significant attack on the austenite was observed from Fig. 5e–l. Fig. 5e showed a very light attack on the austenite/ferrite boundaries and more attack on the austenite.

Gill and Gnanamoorthy [21] have presented the chemical analysis of delta-ferrite which was electrochemically extracted from type 316 weld metal in which molybdenum is present to the extent of 6.15 wt%. The base metal they used contained 2.00 wt% molybdenum, suggesting a three-fold enrichment of molybdenum in the ferrite. From the weld metal chemical analyses we know that the molybdenum contents are 4.16–5.83 wt%. Therefore, one can assume almost 10–15 wt% molybdenum in the weld

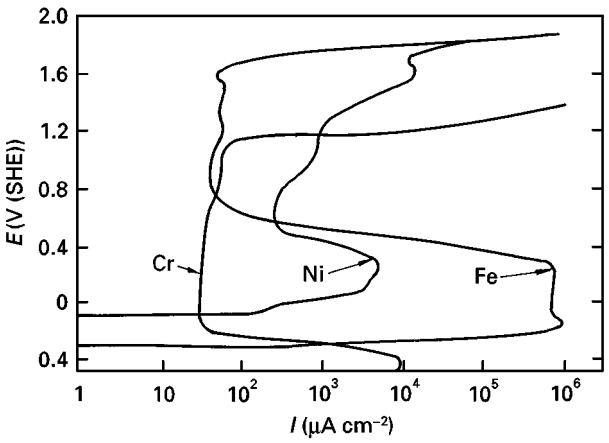

Figure 6 Anodic polarization diagrams of pure chromium, nickel and iron in 1 N H_2SO_4 [13].

metal ferrite under investigation. The electrochemical dissolution behaviour of molybdenum in the alloy form was extensively studied by Greene [15] in sulphuric and hydrochloric acids. The anodic polarization curves of nickel with 5 and 10 wt% molybdenum and Hastealloy F (22.34 wt% Cr, 7.07 wt% Mo) in 1N H_2SO_4 medium are presented in Figs 7 and 8. From these curves one can note that molybdenum, when alloyed, has a very strong bearing on the electrochemical behaviour of an alloy, and is found to affect the shape and position of the active peaks in the polarization curves. The dissolution of delta-ferrite observed at very active potentials was due to chromium-enriched regions, wherein molybdenum-enriched areas

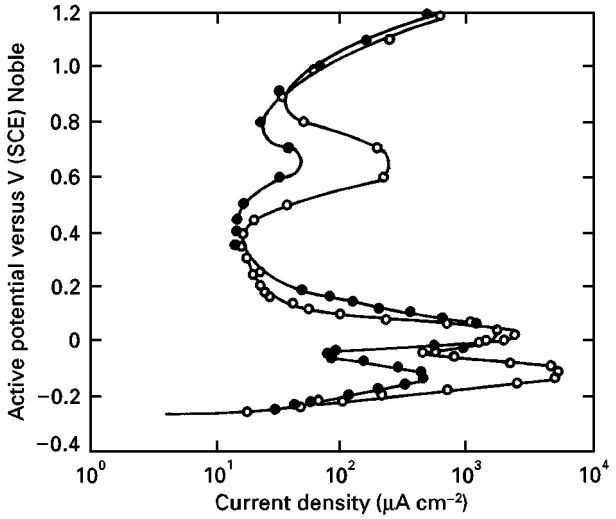

Figure 7 Anodic polarization diagrams of nickel-base alloys containing different quantities of molybdenum in 1 N H_2SO_4 [15]: (○) Ni-5Mo, (●) Ni-10 Mo.

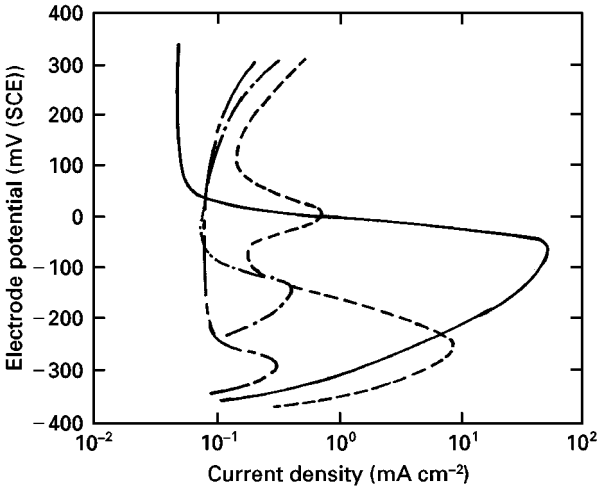

Figure 9 Anodic polarization diagrams of pure delta-ferrite and austenite in 3.6 N H_2SO_4 + 0.1 N NH_4SCN medium [21]: (——) austenite, (– – –) δ-ferrite, (— · —) σ-phase, (— ◦ —) $M_{23}C_6$ carbide.

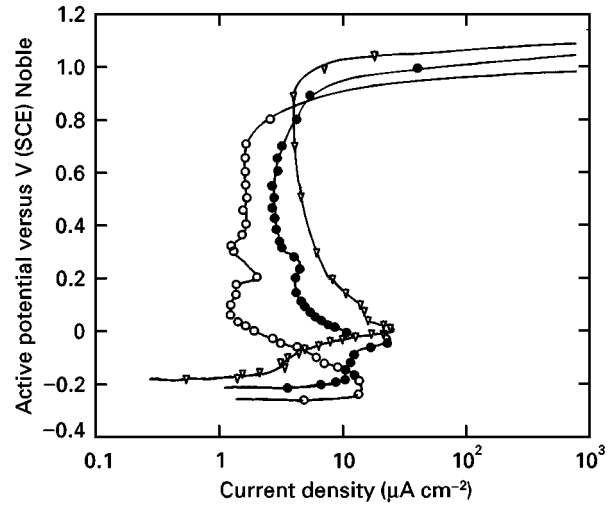

Figure 8 Anodic polarization diagrams of Hastelloy F in sulphuric acid medium [15]: (○) 1 N H_2SO_4, (●) 5 N H_2SO_4, (▼) 10 N H_2SO_4.

had remained cathodically protected and hence inactive. At and above − 360 mV(SCE) the molybdenum-rich zones of ferrite begin to be corroded. Micrographs in Fig. 5f, g and k show these features clearly. The microstructure presented in Fig. 5k, although appearing to be some ferrite, cannot be grouped in any of the accepted standard ferrite morphologies. Gill and Gnanamoorthy [21] have presented the anodic polarization curve of the electrochemically extracted and compacted ferrite, albeit in slightly concentrated sulphuric acid and ammonium thiocyanate (Fig. 9). This curve showed two anodic peaks, the smaller one being located at 0.0 mV(SCE). Depending on the electrochemical medium of study and the chemical composition of the ferrite, the peak positions are expected to change. Essentially one can conclude that the attack on delta-ferrite which took place again from − 360 to − 240 mV(SCE) was due to the enrichment of molybdenum present. Corrosion attack was also observed at δ/γ boundaries as can be seen from the micrographs (Fig. 5h–j). A careful observation of these micrographs revealed that it was the δ/γ boundary which was heavily attacked and the ferrite had the skeletal (Fig. 5b) and lathy (Fig. 5i, j) morphology, the primary cores being extremely fine. Therefore, the attack on the δ/γ boundaries leading to deep grooving on either side of the fine ferrite appeared as though ferrite itself was attacked. In these micrographs, attack on the austenite was also significant, as could be seen from the grey background. Dissolution of the specimen at − 220 mV(SCE) showed a peculiar microstructure presenting a vermicular ferrite-like structure dispersed over the entire matrix. It is known that at these potential delta-ferrites would be totally passive and cannot be observed. Careful observation revealed that ferrite was passivated and was in the background, and etched regions were not ferrite particles. In order to prove this, the specimen was indented at a few places by using a hardness measuring equipment and photographed. Subsequently, it was etched in Murakami reagent which is a specific etchant for ferrite. Fig. 10a showed skeletal ferrite-like microstructure with indentation marks and Fig. 10b the same area after etching the specimen in Murakami reagent whereby ferrite was selectively etched and revealed. The comparison of these micrographs showed that what appeared to be ferrite was actually interdendritic zones which were the last ones to be attacked before the specimen passivated. During solidification, the ferrite formers concentrate in primary ferrite, and austenite formers like nickel are rejected into the liquid. Simultaneous impingement of such liquid with less chromium and nominal or greater amounts of nickel, resulted in what is called interdendritic regions. This effect could be clearly demonstrated by Fig. 10c which showed the boundary between the lower heat input weld and the weld with 75 s melting time. Because the weld with 75 s melting time had very coarse ferrite, it had larger interdendritic zones which were found to be heavily attacked during potentiostatic etching. Another

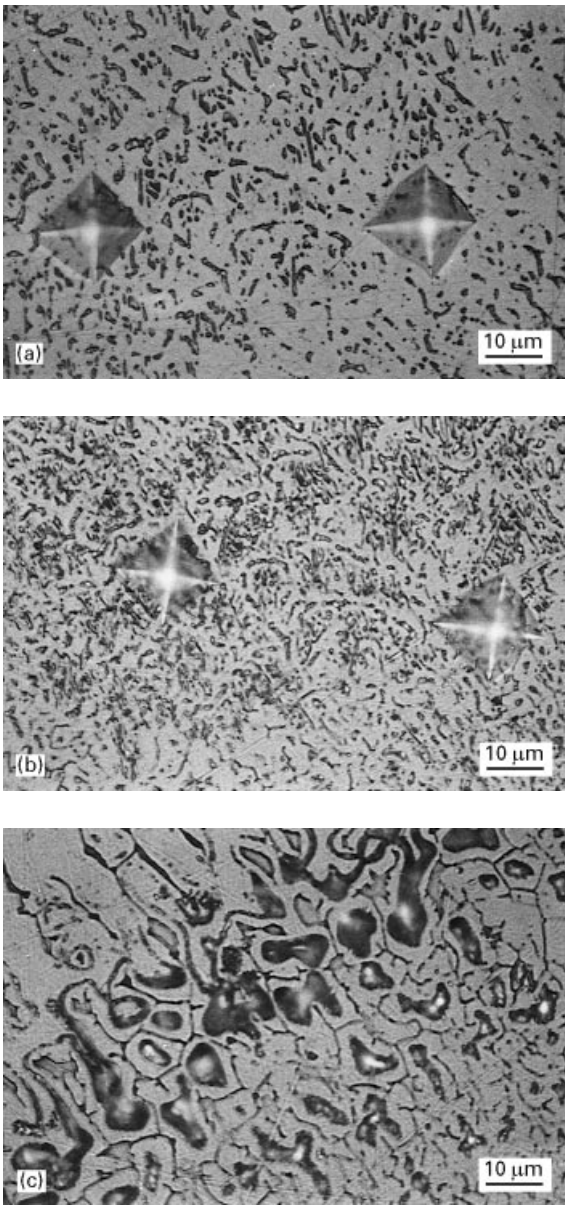

Figure 10 Weld metal specimen: Mo1, 0.36 kJ mm^{-1}. (a) Potentiostatically etched at − 220 mV(SCE), (b) followed by etching in Murakami's reagent. (c) The boundary between 0.36 kJ mm^{-1} weld metal and weld metal with 75 s melting time.

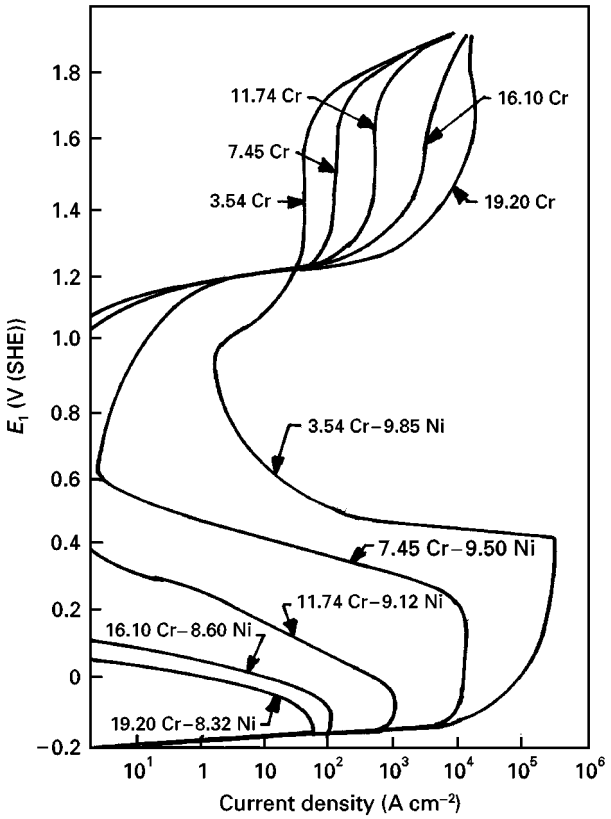

Figure 11 Anodic polarization diagrams of alloys of iron with fixed nickel (~ 9 wt%) and various chromium contents [14].

feature of these micrographs was the areas of ferrite which were immune to attack, while interdendritic regions located at the centre of the ferrite network were attacked. The regions immune to attack at this potential were attacked heavily at very active potentials (− 440 to − 400 mV(SCE)) owing to the very high chromium concentration in these regions. The selective attack on these interdendritic regions at such noble potentials could be explained by using other polarization diagrams [14] wherein each diagram corresponds to a different chromium concentration at constant nickel concentration (Fig. 11). It is clear from Fig. 11 that as the chromium concentration decreased from 19.2 wt% to 3.54 wt%, the active peak current density increased by many orders of magnitude, correspondingly reducing the range of passivity. This led to an increase in the prepassivation or Flade potentials to a more noble value. In fact, the alloy with 3.54 wt% chromium could hardly be passivated. Therefore, etching at − 220 mV(SCE), revealed those areas in the austenite matrix which were depleted in chromium and molybdenum during solidification and subsequent cooling. This effect is termed coring, and is generally higher in molybdenum-containing welds [22]. The reduction of chromium at the austenite cell centres has been studied by Brooks *et al.* [23] on the number of 304L autogenous welds wherein they studied the chromium and nickel concentration profiles across the δ/γ/δ dendrites by scanning transmission electron microscopy (STEM). Etching at − 200 mV(SCE) passivated these specimens.

4. Conclusions

From the above investigations on the molybdenum-containing type 316 stainless steel weld metals (molybdenum content increased from 2.42 wt% to 4.16 and 5.83 wt%, respectively, in two separate groups of weld metals), the following conclusions were drawn.

1. When chemically etched, the weld metals revealed typical delta-ferrite morphology which could be grouped into the standard ferrite morphologies. No other phase or microconstituents was revealed by this etching technique.

2. Delta-ferrite was attacked at very active potentials (− 440 to − 340 mV(SCE)) along with the segregated regions around ferrite which were rich in chromium. In the potential range of − 440 to − 400 mV(SCE), attack on austenite was negligible.

3. Corrosion attack on ferrite in the potential range of -360 to -240 mV(SCE) was attributed to the molybdenum rich areas of ferrite. This was correlated with the typical active dissolution behaviour of molybdenum which, when alloyed with other elements, exhibits its strong influence on the overall dissolution of the alloy.

4. Weld metal dissolution at -220 mV(SCE) was characterized by a microstructure which though appearing like ferrite was actually found to be due to the dissolution of the interdendritic regions of the weld metals which were depleted in chromium.

Acknowledgements

The authors thank Dr V. S. Raghunathan, Head, Metallurgy Division, IGCAR, Kalpakkam, for his constant encouragement, and Dr Baldev Raj, Director, Metallurgy and Materials Group, Kalpakkam, for his keen interest in this work.

References

1. F. C. HULL, *Weld. J.* **46** (1967) 399s.
2. A. GARNER, *Corrosion* **35** (1979) 108.
3. O. HAMMAR and U. SVENSON, "Solidification and Casting of Metals" (The Metals Society, London, 1979) p. 401.
4. R. A. FARRAR, in "Stainless Steels' 84" (The Institute of Metals, London, 1986) p. 336.
5. M. LINDENMO, *ibid.* p. 262.
6. M. J. CIESLAK and W. F. SAVAGE, *Weld. J.* **60** (1981) 131s.
7. T. G. DAVEY, T. G. GOOCH and J. L. ROBINSON, *Metal Construct.* (1987) 545.
8. T. G. GOOCH, *Weld. Metal Fabric.* April (1990) 5.
9. T. G. GOOCH, J. HONEYCOMBE and P. WALKER, *Br. Corros. J.* **6** (1971) 148.
10. V. CIHAL and M. PRAZAK, *J. Iron Steel Inst.* (1959) 360.
11. P. I. MARSHALL and T. G. GOOCH, *Corrosion* **49** (1993) 514.
12. T. G. GOOCH, *Weld. Inst. Res. Bull.* **15** (1974) 183.
13. R. L. BEAUCHAMP, PhD dissertation, The Ohio State University, Columbus, OH (1966).
14. K. OSAZAWA and H. S. ENGEL, *Corros. Sci.* **6** (1966) 389.
15. N. D. GREENE, in "Proceedings of the First International Congress on Metallic Corrosion", (Butterworths, London, 1962) I.11, 113.
16. N. SUUATALA, T. TAKALO and T. MOISIO, *Metall. Trans.* **11A** (1980) 717.
17. S. A. DAVID, *Weld. J.* **60** (1981) 63s.
18. J. A. BROOKS and A. W. THOMPSON, *Int. Mater. Rev.* **36** (1991) 16.
19. J. C. LIPPOLD and W. F. SAVAGE, in "Modeling of Casting and Welding Processes", edited by H. Brody and D. Apelian (Metallurgical Society of ASME, Warrendale, PA, 1981) p. 443.
20. J. A. BROOKS and M. J. BASKES, in "Advances in Welding Science and Technology", edited by S. A. David (ASM International, Metals Park, OH, 1987) p. 93.
21. T. P. S. GILL and J. B. GNANAMOORTHY, *J. Mater. Sci.* **17** (1982) 1513.
22. A. GARNER, *Corrosion* **35** (1979) 108.
23. J. A. BROOKS, J. C. WILLIAMS and A. W. THOMPSON, *Metall. Trans.* **14A** (1983) 1271.

Received 20 September 1996
and accepted 27 January 1998